5-7-2020

Dynamic Tasks and Developmental Dysplasia of the Hip

Elizabeth Saliba
Washington University in St. Louis

Washington University in St. Louis
Department of Mechanical Engineering
MEMS 400 Independent Study
April 23, 2020

Dynamic Tasks and Developmental Dysplasia of the Hip

Written by: Elizabeth Saliba
Faculty Advisor: Dr. Michael D. Harris

Introduction

This semester, I worked in Dr. Michael Harris' Orthopaedic Biomechanics lab which studies bone-muscle relationships in patients with developmental dysplasia of the hip (DDH). DDH is a condition where the femoral head does not fit correctly into the pelvis. In DDH patients, the hip is characterized by bony abnormalities of the acetabulum and femur which can lead to soft tissue damage of the articular cartilage and acetabular labrum [1-3]. This congenital condition forms in early development, and its effects are exaggerated by high activity levels in adolescence and young adulthood [3]. If left untreated, soft tissue damage develops to osteoarthritis (OA) and eventually may require total joint replacement [4].

While muscle function likely contributes to DDH symptoms, the role of muscles is not well understood in DDH pathomechanics. Current treatment for DDH patients considers the bone and muscle separately rather than understanding their relationship. The treatment focuses on repairing bony abnormalities and aims to provide mid- to long-term joint preservation [5, 6]. Moreover, it does not guarantee elimination of symptoms, restoration of activity, or prevention of OA. Current pre- and post-treatment rehabilitation strategies involve general muscle strengthening, but it lacks the precision needed to understand how the bony abnormalities affect the surrounding muscles of the hip region [7-10]. Therefore, the overall objective of this research is to develop an understanding of bone-muscle relationships and their effect on symptomatology, hip mechanics, and joint damage with a long-term goal of optimizing DDH treatment strategies.

To contribute to the long-term goal of Dr. Harris's lab, the primary objective of this semester's research was to analyze patients performing high demand dynamic tasks (e.g. running, squatting, and cutting) using rigid-body dynamics modeling in Vicon Nexus and in-vivo 3D motion capture in Visual 3D. With this data, movement patterns were compared between healthy individuals and DDH patients through an analysis of lower-extremity joint moments and angles while performing hop-and-cuts, and the results are presented here. The data processed for running, squatting, and run-and-cuts will be used in future musculoskeletal models.

Methods

The methods used to analyze the movement patterns of patients performing dynamic tasks are described in full detail here.

Rigid Body Dynamic Modeling

In Dr. Harris's Lab, live data was collected using Vicon Nexus by placing markers on the patient to distinguish locations on the body. Figure 1 visualizes the label and location assigned to each of the 70 markers.

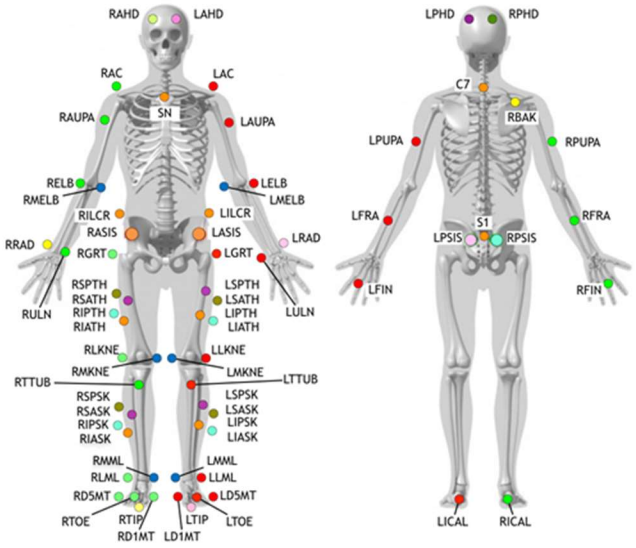

Fig. 1 Diagram of patient with labelled markers for Vicon data processing [11].

Located in the center of the lab were a treadmill and ground force plates, which were used to record the mass of the patient and ground force reactions. The patient performed calibration, range of motion, functional hip, walking, and running trials on the treadmill, and squatting, run-and-cutting, and hop-and-cutting on the ground force plates. While the patient performed various tasks, ten cameras set up around the perimeter of the lab detected the markers, and these recordings were combined to create rigid-body models. While static trials included all 70 markers indicated in Fig. 1, dynamic trials included 66 markers, removing the medial leg markers (LMKNE, RMKNE, LMML, RMML). This was done to ensure motion during dynamic trials was not altered by the patient trying to prevent the markers from colliding.

The data from live collection was exported to Vicon Nexus, where I was responsible for ensuring that all models were labelled fully and correctly. The calibration for each trial required each trajectory to be manually labeled, and this file was used when constructing subsequent models for that patient. For each trial, the "reconstruct and label" pipeline was initially run, which labelled a portion of the model as fit with the underlying code specifications. However, due to phantom markers resulting from reflections on the patient and markers overlapping with each other from the camera's perspective, it was necessary to scroll through the time bar and un-

label any incorrectly labeled trajectories and delete any phantom markers. Typical issues that resulted from this pipeline included mislabeling between the medial elbow and iliac crest during squatting and the greater trochanter and acetabulum when cutting. Once this step was complete, the Woltring filter was run, which filled gaps in the model to the best of the pipeline's ability. Again, scrolling through the time bar was critical to ensure the pipeline did not create any incorrect labels. To fill the remaining gaps, the "pattern fill" and "rigid body fill" were used. Pattern fill was used to identify the path of a missing trajectory by selecting a source trajectory to mimic. Rigid body fill was used for thigh and calf plates characterized by four markers - when one marker was missing from these plates, the three apparent markers were selected as sources to fill the gap.

After labelling, it was important to verify the quality of the model. Vicon provided a quality assessment tool to monitor the labeling process, indicating the percentage of markers labeled and number of gaps. While a fully labeled dynamic model had zero gaps, it only had 94% of markers labeled due to the previously mentioned removal of medial leg markers. A graph of the number of trajectories over the course of the trial was used to verify the quality assessment. An example of a fully labeled dynamic model from a hop-and-cut trial is pictured in Figure 2.

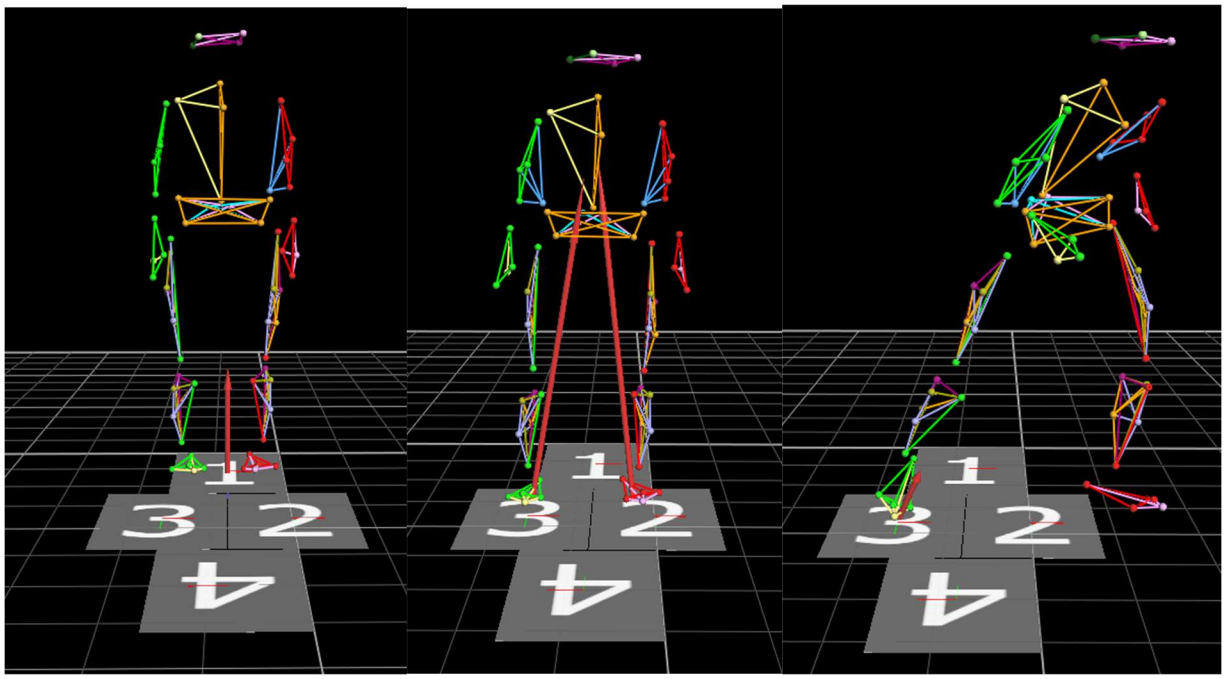

Fig. 2 **Rigid-body dynamic model of patient performing a hop-and-cut. Red arrows signify ground reaction forces.**

In-Vivo 3D Motion Capture

When a trial was saved in Vicon Nexus, its corresponding C3D file was exported. The C3D files were uploaded to Visual 3D and organized by activity for each patient (e.g walk, run squat, and cut workspaces). The squat workspaces included data for both single-leg and double-leg squats, and the cut workspaces included data for both run-and-cuts and hop-and-cuts. Along with each activity, the calibration, range of motion, and functional hip files were included in each workspace. The mass calculated from the ground force plates and height of each patient were specified to ensure accuracy when analyzing the models. By creating workspaces for each activity, time was optimized so the files could be processed and saved most efficiently. Both generic and subject specific workspaces were created. For the purposes of my independent study, I focused on the subject specific workspaces that utilized MRI data to locate the hip joint center of each patient, allowing for more individualized joint moment and angle calculations.

To ensure quality joint moment and angle calculations, the most effective frequencies at which lowpass filters could be run to filter out high frequency noise while preserving significant data points were determined. Table 1 includes the optimal cutoff frequencies determined for processing lowpass filters across the analog signals and trajectory components.

Table 1: Processing frequencies for lowpass filters

Workspace	Force cutoff frequency (Hz)	Trajectory cutoff frequency (Hz)
Run	20	8
Squat	10	6
Cut	25	8

These frequencies were used to provide a consistent filter range from patient to patient, but were adjusted as necessary after analyzing joint moments. The filter and calculation pipelines were executed according to where data was recorded. The “Filter_ComputeJointAnglesandMoments_ TreadmillRun” pipeline was used for processing run workspaces, and the “Filter_ComputeJoint AnglesandMoments_GroundFP” pipeline was used for processing squat and cut workspaces.

Trial data that captured the specific activity of interest were denoted by placing start and stop tags at time points corresponding to positions that were distinguishable across all patients. These locations removed insignificant data while providing uniformity across all patients, and they were determined through an analysis of force components and trajectory paths. While a

'gait events detection' tool automatically provided labels for heel-strikes and toe-offs for the entirety of each trial, the other tasks required manual labeling. The dynamic tasks, their respective start and stop locations, and the criteria for identifying the locations are included below with corresponding figures:

Single-leg/double-leg squats

- Start location: Maximum S1 z-location immediately prior to knee bending on squat leg
- Stop location: Maximum S1 z-location after squatting motion

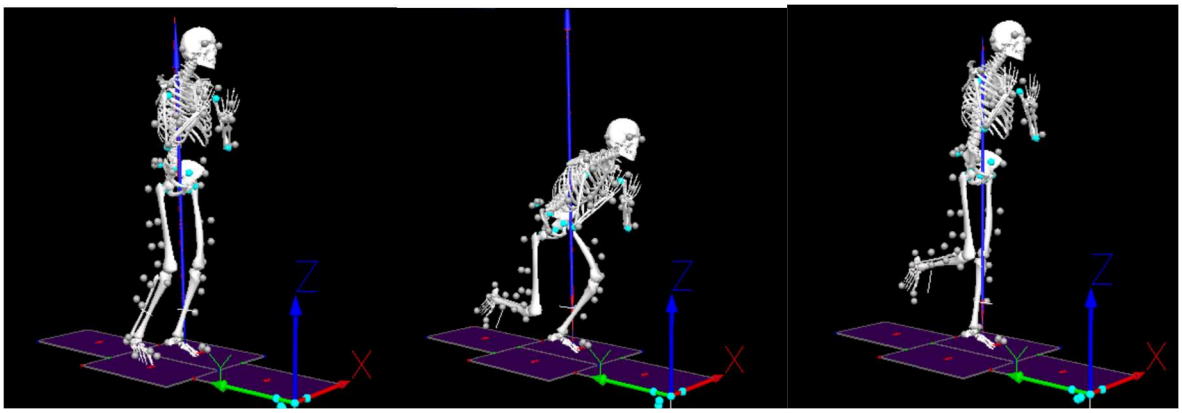

Fig. 3 Rigid-body dynamic model of patient performing a single-leg squat at its start location (left), mid-squat (center), and stop location (right).

Hop-and-cuts

- Start location: First frame when ground reaction forces detected by both feet
- Stop location: Frame immediately after final force detection of trail leg

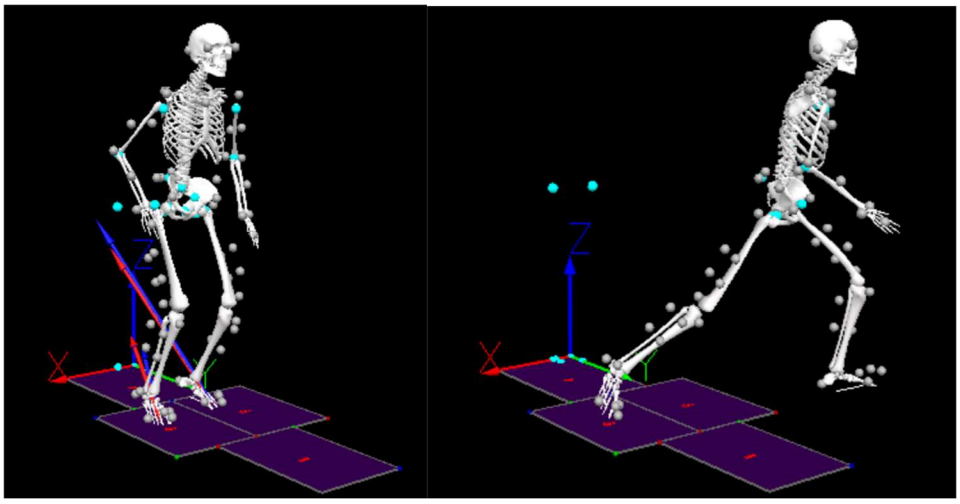

Fig. 4 **Rigid-body dynamic model of patient performing a hop-and-cut at its start (left) and stop (right) locations.**

Run-and-cuts

- Start location: First frame when ground reaction forces detected by force plate 4
- Stop location: Frame immediately after final force detection

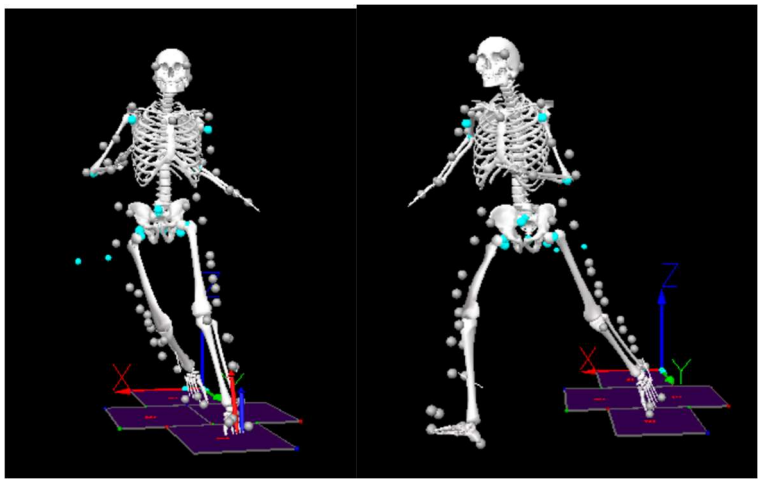

Fig. 5 **Rigid-body dynamic model of patient performing a run-and-cut at its start (left) and stop (right) locations.**

Calculation of Joint Angles and Moments

Moving forward in the independent study, hop-and-cuts were studied in further depth. The purpose of understanding the joint moments and angles when performing hop-and-cuts was to provide a method of comparison between healthy individuals and DDH patients during an activity that challenges subjects' range of motion. More specifically, the joint moments and angles of healthy individuals cutting with their dominant leg as the trail leg were compared with those of DDH patients cutting with their symptomatic leg as the trail leg. Moments and angles were calculated about the trail leg's ankle, hip, and knee in the x, y, and z directions using Visual3D pipelines. Joint angles were reported as the position of the distal segment relative to the proximal segment and calculated using a 6 degree-of-freedom position optimization algorithm based on the position of the markers on each body segment. For instance, the hip angle represented the position of the femur relative to the pelvis, centered at the subject specific hip joint center. Joint moments were calculated using inverse dynamics based on the joint angles and

the scaled inertial parameters of each individual segment. Segment angles (meaning the position of a segment relative to the lab coordinate systems) were also calculated about the individual's pelvis.

To export data from Visual 3D to MATLAB, code (contained in Visual 3D pipelines) initially written for exporting joint moments and angles for walking activities was adapted for hop-and-cuts. Using the start and stop labels, the pipeline time normalized the joint angles and moments of each activity to provide 101 data points for each trial. In live data collection, at least three trials were conducted of the individual cutting to the left and at least three cutting to the right. Since the analysis focused on the dominant leg of healthy individuals and symptomatic leg of DDH patients, averages of three trials for both moments and angles were only taken about the leg of interest. The standard deviations across all healthy individuals and all DDH patients was calculated and considered when interpreting the data.

Joint Angles and Moments

While data was collected for analysis of ankle, knee, hip, and pelvis joints, the remainder of this report focuses on hip joint angles and moments. More specifically, this data provides a comparison between healthy individuals with a dominant right side and DDH patients with a symptomatic right side. The healthy individuals in the category of right-side dominance were assessed through data collected for the x-, y-, and z- components of the hip joint moments and angles when hop-and-cutting. The same assessment was performed on DDH patients with right side symptoms. The healthy individuals complying with these standards were addressed as the control group, and the DDH patients were addressed as the experimental group.

The coordinate system designated in Visual 3D corresponded with clinical planes that were critical to recognize when interpreting the data. The positive x-direction corresponded with hip flexion while the negative x-direction corresponded with hip extension. The positive y-direction corresponded with hip adduction while the negative y-direction corresponded with hip abduction. The positive z-direction corresponded with external hip rotation while the negative z-direction corresponded with internal hip rotation. An understanding of these coordinates was only applicable if uniform start and stop locations were assigned across trials; otherwise, the time normalized data would not average proportionally and subsequently skew the data. Hop-and-cuts were an activity that generally had variation across patients and even among the trials of an

individual patient due to spontaneity when performing the task. For a more natural response, patients were randomly signaled which direction to cut towards while hopping. Therefore, there was a less repetitive pattern in the data for this task when compared to squatting and running. As a result, identifying uniform start and stop locations for this task was an important part of this independent study.

For all graphs included in this report, the data at time point 0 represented the previously described start location corresponding to hop-and-cutting, and the data at time point 101 represented the stop location. By graphing the individual sets of data for each subcategory, these assessments provided reason to use the average among the patients of each group by verifying the expected general trend when plotted individually on the same graph. However, it was important to recognize the range of starting points, which subsequently shifted the trend along the y-axis. Graphs used for analysis of the x-components of hip joint angles for both healthy individuals and DDH patients are pictured below in Figure 6 to recognize the varying starting values.

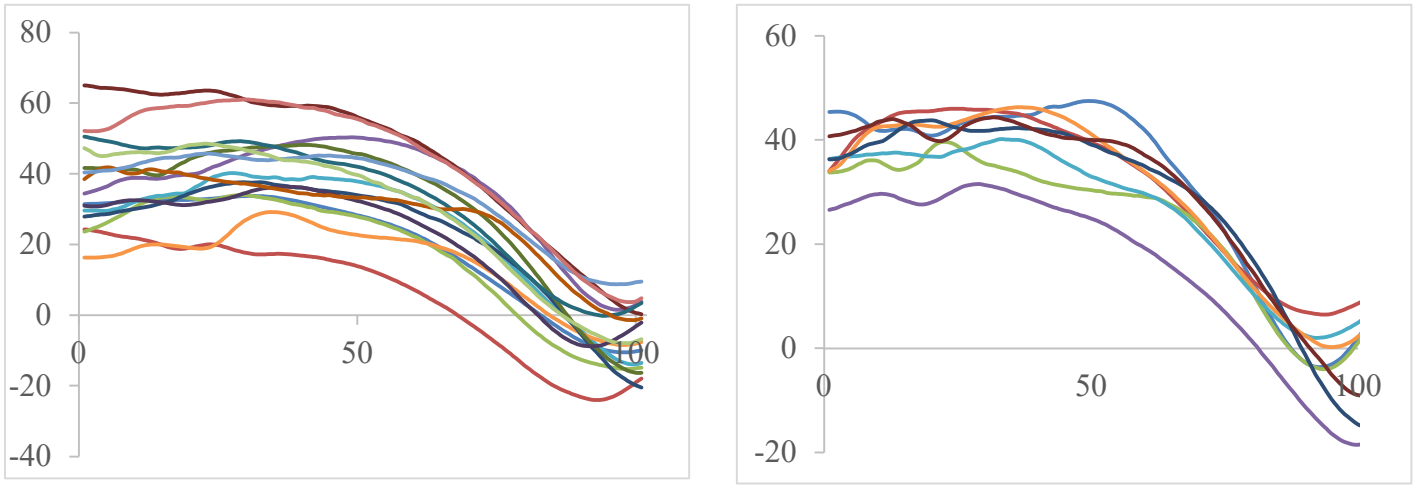

Fig. 6 X-components of hip joint angles of healthy individuals (left) and DDH patients (right).

The discrepancies among starting angles require further analysis within the hop-and-cut trials of a single patient. This was likely attributed to slight variations in the landing pattern that indicated the start location of the trial. For instance, very few patients landed with both feet simultaneously during the initial hop; rather, one foot followed another within a short time frame. Therefore, the varying start angles could be a result of one patient's right foot planted on

the force plate for a different amount of time than other patients. The hip joint moments also displayed varying values in the initial time frame, and the data was quite noisy, even before averaging. The following graphs visualize the average moment data across individual patients corresponding to the x-components of hip joint moments for both healthy individuals and DDH patients.

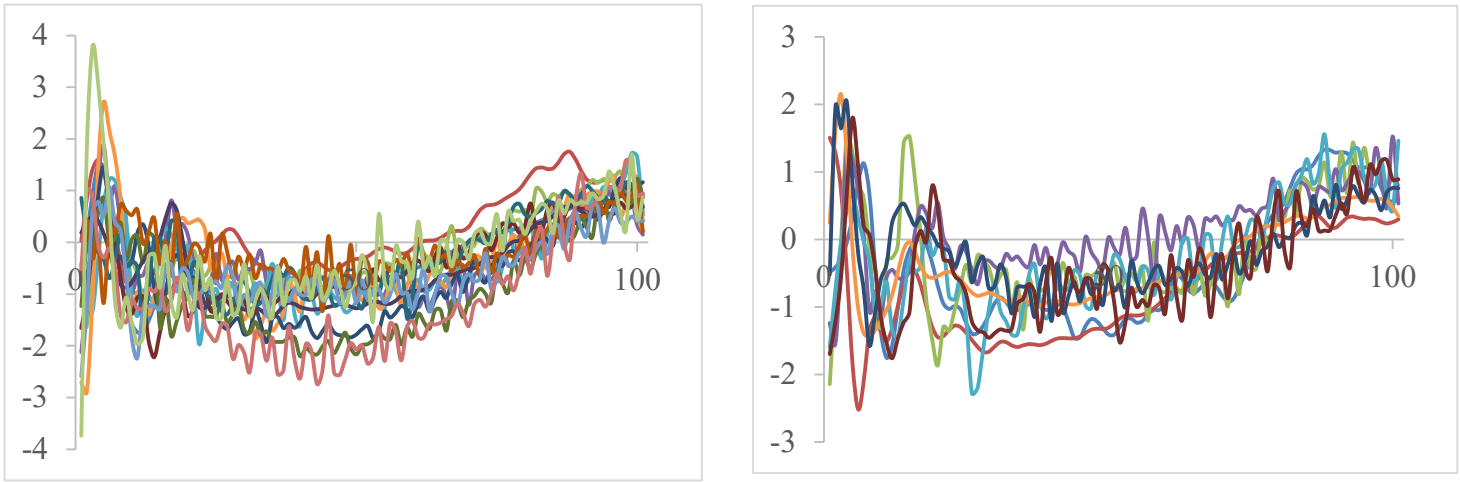

Fig. 7 X-components of hip joint moments of healthy individuals (left) and DDH patients (right).

Another important task of this independent study was to identify cutoff frequencies for both forces and trajectories when running the lowpass filter to calculate joint angles and moments. The noise in Figure 7 was attributed to a high cutoff frequency that allowed for residual noise to obscure the true signal. However, this noise was unexpected since the force plates on which the task was performed were mounted into the ground. When filtering the forces at a lower cutoff frequency, the filter removed a critical peak. Therefore, we can assume that the ideal force cutoff frequency for filtering the moment data falls somewhere within the range of 10 Hz to 25 Hz. Since the angle data appeared smooth, the V3D pipeline should be divided into separate moment and angle calculations since the graphs suggest that the filtering cutoff for marker trajectory data (i.e. the signals that determine joint angles) was sufficient.

A 2-independent sample t-test was performed on each angle and moment component (x, y, and z) by identifying the maximum and minimum moments and angles of each patient and calculating the mean $\bar{X}$ and standard deviation s of these extrema within the control and DDH groups. The sample size of the healthy individuals was 15, and the sample size of the DDH

patients was 8. The calculated p-value was used to assess significant differences between the healthy individuals and DDH patients. The results of this test are included in the tables below.

Table 2: 2-Independent Sample t-Test on Maximum Hip Joint Angle

	Healthy $\bar{X}$	Healthy *s*	DDH $\bar{X}$	DDH *s*	p-value
X	43.113	11.266	42.428	5.213	0.873
Y	-5.272	3.580	-4.570	3.531	0.658
Z	0.097	12.428	-2.174	5.431	0.630

Table 3: 2-Independent Sample t-Test on Minimum Hip Joint Angle

	Healthy $\bar{X}$	Healthy *s*	DDH $\bar{X}$	DDH *s*	p-value
X	-7.505	9.467	-5.172	8.536	0.567
Y	-24.256	6.351	-22.924	4.908	0.612
Z	-24.914	9.333	-25.212	7.236	0.938

Table 4: 2-Independent Sample t-Test on Maximum Hip Joint Moment

	Healthy $\bar{X}$	Healthy *s*	DDH $\bar{X}$	DDH *s*	p-value
X	1.608	0.758	1.686	0.286	0.784
Y	1.035	0.229	1.066	0.309	0.792
Z	0.480	0.166	0.546	0.134	0.352

Table 5: 2-Independent Sample t-Test on Minimum Hip Joint Moment

	Healthy $\bar{X}$	Healthy *s*	DDH $\bar{X}$	DDH *s*	p-value
X	-2.086	0.680	-1.875	0.389	0.430
Y	-1.031	0.331	-1.052	0.183	0.869
Z	-0.817	0.238	-0.736	0.151	0.396

With an initial null hypothesis that the $\bar{X}$ values for healthy individuals and DDH patients would be equal, the large p-values calculated across the maximum and minimum hip joint moments and angles indicated that the evidence was too weak to reject this hypothesis. Visualizing the graphs of the average x-, y-, and z- components of hip joint angles during hop-and-cuts contributed to verifying the conclusions drawn through the t-test. The minimum and

maximum values corresponding to the healthy and DDH groups for Figures 6, 7, and 8 can be found in Tables 2 and 3.

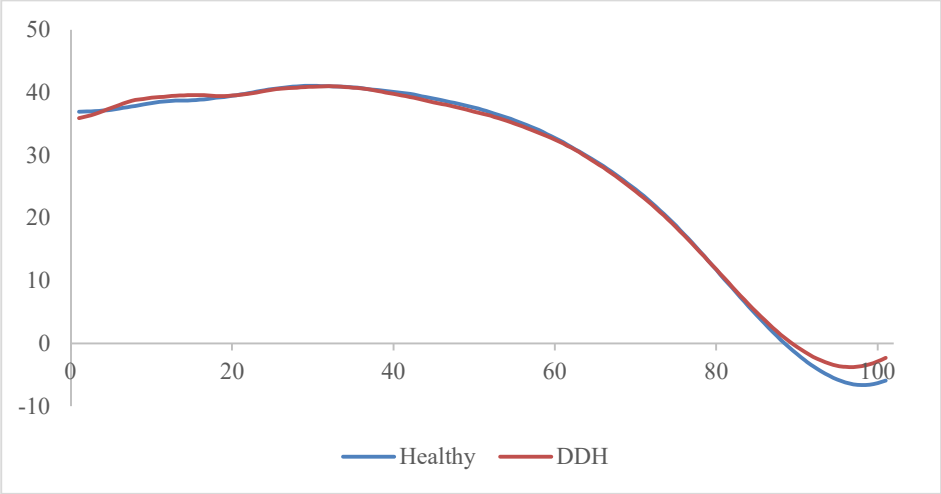

Fig. 8 **Comparison between average x-component of hip joint angles of healthy individuals and DDH patients**

Figure 8 indicated there were no major differences between the maximum x-component of the hip joint angle for the two groups. However, the minimum x-component of the healthy hip joint angle appeared to reach a value of -6.614 degrees while the DDH patient only reaches -3.752 degrees. This angle difference occurred when the subject was pushing off the force plate, corresponding with a slightly greater degree of hip joint extension. However, the difference is not substantial enough to draw any significant conclusions.

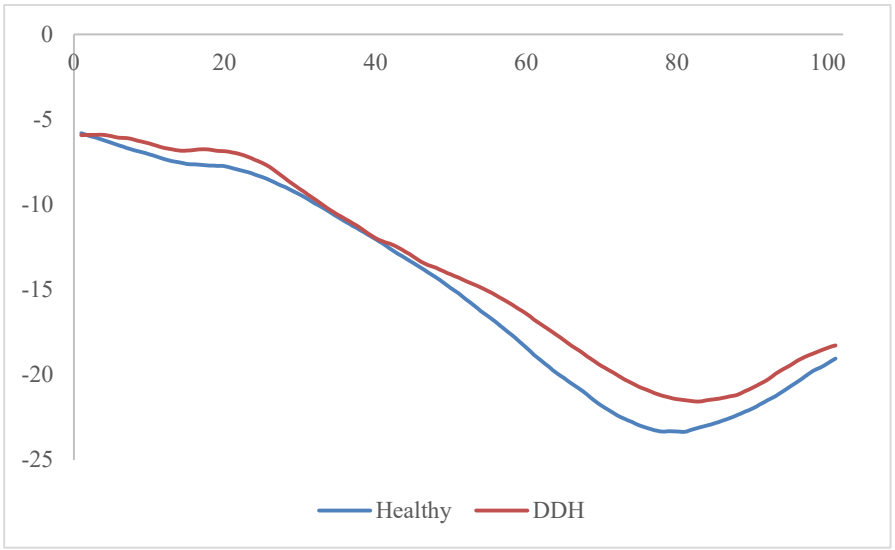

Fig. 9 **Comparison between average y-component of hip joint angles of healthy individuals and DDH patients**

Like the x-component, Figure 9 did not show major differences between the maximum y-component of the hip joint angle corresponding to hip abduction. The y-component of the healthy hip joint angle reached a minimum value of -23.338 degrees while the DDH hip joint angle -21.570 degrees. This data confirmed that the healthy individual and DDH patient did not display significant differences in hip joint adduction.

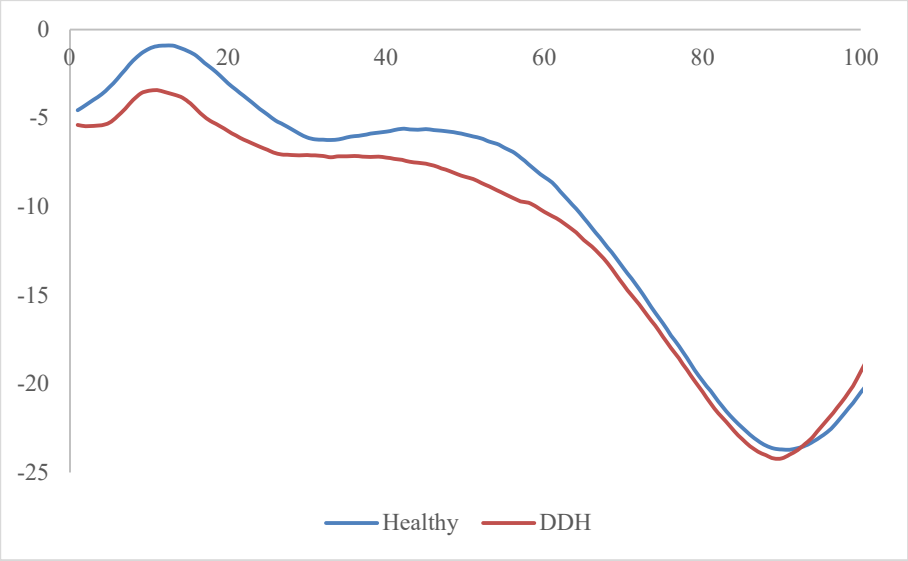

Fig. 10 Comparison between average z-component of hip joint angles of healthy individuals and DDH patients.

Figure 10 indicated a slight difference between the maximum z-components of the healthy and DDH hip joint angles, which occurred soon after the initial hop motion. Again, the healthy individual appeared to exhibit a slightly greater external hip rotation with a z-component joint angle of -0.911 degrees while the DDH joint angle measured -3.428 degrees.

Conclusion and Future Steps

From the statistical analysis of hip joint angles during hop-and-cuts, there seemed to be no significant difference between the movement of healthy individuals and DDH patients. The inconsistency in moment data for both groups prevented any conclusions from being drawn in regard to rotation about the hip joint center.

While the data corresponding to hip joint angles during hop-and-cuts provided smooth curves, the moment data was quite noisy despite the force plates being mounted in the ground. A possible solution to this issue could be to alter the initial filter for computing joint angles and moments into two separate pipelines in V3D. As a result, a suitable cutoff frequency can be

identified for more precise moment data without altering the angle data. To gain a better understanding of the various angles and moments in the initial time frame, the start location should be analyzed among trials of an individual patient to determine if there is a more uniform position that could standardize the data.

References

[1] Henak CR, Ellis BJ, Harris MD, et al. 2011. Role of the acetabular labrum in load support across the hip joint. J. Biomech.

[2] Clohisy JC, Knaus ER, Hunt DM, et al. 2009. Clinical presentation of patients with symptomatic anterior hip impingement.Clin. Orthop. Relat. Res. 467(3):638–644.

[3] Nunley RM, Prather H, Hunt D, et al. 2011. Clinical presentation of symptomatic acetabular dysplasia in skeletally mature patients. [Internet].J. Bone Joint Surg. Am. 93 Suppl 2:17–21Available from: http://www.ncbi.nlm.nih.gov/pubmed/21543683.

[4] Wyles CC, Heidenreich MJ, Jeng J, et al. 2016. The John Charnley Award: Redefining the Natural History of Osteoarthritis in Patients With Hip Dysplasia and Impingement.Clin. Orthop. Relat. Res. :1– 15.

[5] Steppacher SD, Tannast M, Ganz R, Siebenrock KA. 2008. Mean 20-year followup of bernese periacetabular osteotomy.Clin. Orthop. Relat. Res. 466(7):1633–1644.

[6] Garras DN, Crowder TT, Olson S a. 2007. Medium-term results of the Bernese periacetabular osteotomy in the treatment of symptomatic developmental dysplasia of the hip.J. Bone Joint Surg. Br. 89(6):721–724.

[7] Schmerl M, Pollard H, Hoskins W. 2005. Labral injuries of the hip: A review of diagnosis and management.J. Manipulative Physiol. Ther. 28(8):1–8.

[8] Hunt D, Prather H, Hayes MH, Clohisy JC. 2012. Clinical Outcomes Analysis of Conservative and Surgical Treatment of Patients With Clinical Indications of Prearthritic, Intra-articular Hip Disorders [Internet].Pm&R 4(7):479–487Available from: http://dx.doi.org/10.1016/j.pmrj.2012.03.012.

[9] Margo K, Drezner J, Motzkin D. 2003. Evaluation and management of hip pain: an algorithmic approach.J. Fam. Pract. 52(8):607–617.

[10] Adler KL, Cook PC, Geisler PR, et al. 2015. Current Concepts in Rehabilitation After Hip Preservation Surgery Part II [Internet].Sport. Heal. A Multidiscip. Approach 14642(C):57–64 Available from: http://sph.sagepub.com/content/early/2015/04/28/1941738115577621.abstract.

[11] Song K, Harris MD, Krull, C, et al. 2017. Data Processing in Vicon Nexus.

[12] “SPSS Tutorials: Independent Samples t Test,” 2020, Kent State University, from https://libguides.library.kent.edu/SPSS/OneSampletTest

Acknowledgements

I would like to express my gratitude to Dr. Michael Harris for giving me the opportunity to work in his lab and develop a new understanding of mechanical engineering in the field of physical therapy. Dr. Harris allowed me to gain experience with several methods of 3D in-vivo motion capture and analysis, and he did so in a way where I understood the significance of my work. I would also like to thank Ke Song, Molly Shepherd, and Brecca Gaffney for being readily available to provide guidance over the course of the semester.